

## **Part II Applied Physics**

Section 1 Atomic, Molecular and Optical Physics

Section 2 Plasma Physics

Section 3 Electromagnetics

Section 4 Radio Astronomy



## **Section 1 Atomic, Molecular and Optical Physics**

Chapter 1 Quantum Optics and Photonics

Chapter 2 Basic Atomic Physics



# Chapter 1. Quantum Optics and Photonics

## Academic and Research Staff

Professor Shaoul Ezekiel

## Visiting Scientists and Research Affiliates

Dr. Philip R. Hemmer,<sup>1</sup> Dr. Mara G. Prentiss,<sup>2</sup> Dr. Elias Snitzer,<sup>3</sup> John D. Kierstead<sup>1</sup>

## Graduate Students

John J. Donoghue, M. Selim Shahriar, Stephen P. Smith, Farhad Zarinetchi

## Technical and Support Staff

Margaret M. McCabe

## 1.1 Error Sources in a Fiber Optic Resonator Gyroscope

### Sponsor

Charles S. Draper Laboratories  
Contract DL-H-418468

Various forms of optical inertial rotation sensors based on the Sagnac effect have been under development since the advent of the laser in 1960. These include active techniques, such as the ring laser gyro<sup>4</sup> and passive techniques employing ring resonators<sup>5</sup> or interferometers.<sup>6</sup> In the past few years, low-loss single-mode optical fibers have been incorporated into both interferometers<sup>7</sup> and resonators.<sup>8</sup> Here, we describe some error sources of a fiber-optic resonator inertial rotation sensor that has been under study in our laboratory.

In the presence of an inertial rotation rate  $\Omega$  normal to the plane of a ring cavity, the nonreciprocal phase shift induced by the Sagnac effect<sup>9</sup> causes the cavity resonances in the clockwise (CW) and counterclockwise (CCW) directions to be separated by a frequency  $\Delta f$  given by

$$\Delta f = \frac{4A}{\lambda P} \Omega \quad (1)$$

where  $A$  is the area enclosed by the resonator,  $P$  is the optical perimeter, and  $\lambda$  is the wavelength of the light.

In order to measure  $\Delta f$  in a passive resonator, two counterpropagating beams are introduced into the cavity and the frequency of each beam is adjusted to coincide with the center of the corresponding cavity resonance. Thus, the frequency difference

<sup>1</sup> Rome Air Development Center, Hanscom Air Force Base, Bedford, Massachusetts.

<sup>2</sup> Professor, Harvard University, Cambridge, Massachusetts.

<sup>3</sup> Professor, Rutgers University, New Brunswick, New Jersey.

<sup>4</sup> A.H. Rosenthal, "Regenerative Circulatory Multiple Beam Interferometry for the Study of Light Propagation Effects," *J. Opt. Soc. Am.* 52: 1143 (1962).

<sup>5</sup> S. Ezekiel and S.R. Balsamo, "Passive Ring Resonator Laser Gyroscope," *Appl. Phys. Lett.* 30: 478 (1977).

<sup>6</sup> W.R. Carrington and R. Fredricks, *Development of an Optical Rate Sensor*, Final Report to the U.S. Navy Office of Naval Research N00014-73-C-0377, Lear Siegler, Inc., Grand Rapids, Michigan, November 1973.

<sup>7</sup> V. Vali and L.W. Shorthill, "Fiber Ring Interferometer," *Appl. Opt.* 15: 1099 (1976).

<sup>8</sup> R.E. Meyer and S. Ezekiel, "Fiberoptic Resonator Gyroscope," presented at the IEE First International Conference on Optical Fiber Sensors, London, April 26-28, 1983.

<sup>9</sup> E.J. Post, "Sagnac Effect," *Rev. Mod. Phys.* 39: 475 (1967); H.J. Arditty and H.C. Lefevre, "Sagnac Effect in Fiber Gyroscopes," *Opt. Lett.* 6: 401 (1981).

between the two beams is simply  $\Delta f$  and is directly proportional to the rotation rate, as shown in equation 1. Figure 1 shows simplified gyro setups for a cavity in reflection (top) and for a cavity in transmission (bottom).

In order to hold each beam at the center of a cavity resonance, the frequency of each beam is modulated before it enters the cavity.<sup>10</sup> After emerging from the cavity, the beams fall on a detector whose signal is demodulated with a phase sensitive detector (PSD) to yield a discriminant which has a zero crossing at the center of the resonance, and this is used by the servo to hold the beam at the cavity resonance.

In practice, there are other sources of nonreciprocal phase shifts besides the Sagnac effect that constitute error sources in the gyroscope, and these must be drastically reduced, if not eliminated, to achieve ultimate performance. Here, we will discuss some of the major error sources and the research that is currently underway.

One major source of error is the coupling of the counterpropagating beams through backscattering from either inside or outside the cavity. This coupling between the two beams will cause a "dead zone" for a range of small rotation rates, similar to that observed in the bulk-optic ring laser gyro.<sup>11</sup>

One method of eliminating this effect is to "wash out" the interference between the beams by sinusoidally modulating the frequency of one of the beams so that its  $J_0$  components are suppressed.<sup>10</sup> In this way, the interference between the beams occurs around the harmonics of the modulation frequency, where it can be easily removed by suitable filtering.

However, even with the interference between the two beams washed out, the residual intensity backscattering still can cause problems by affecting the servo loops if both directions use the same modulation frequency. To avoid the effects of intensity backscattering, different modulation frequencies need to be used in the two directions.<sup>12</sup>

Another error source is due to lineshape asymmetry, caused by loss in the coupler for a cavity in reflection. For example, when different

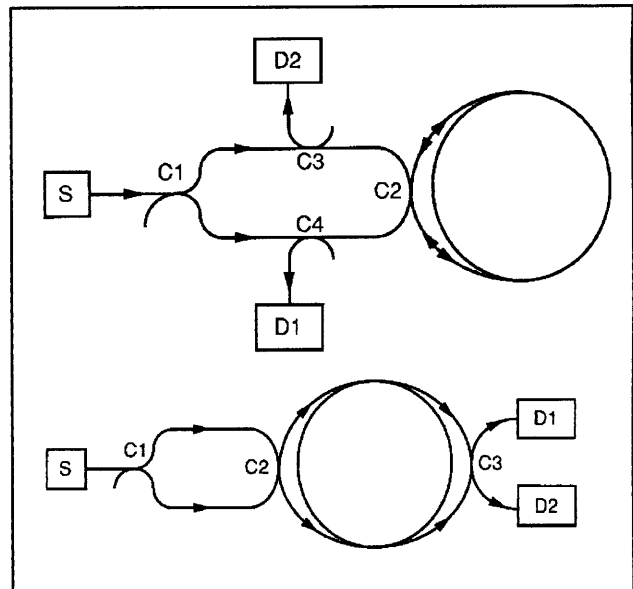


**Figure 1.** Simplified schematic of a ring resonator gyroscope using a resonator in reflection (top) and transmission (bottom).

modulation frequencies are used, the zero crossing of the discriminants in each direction are dependent on the exact parameters of the applied modulation. In this way, an offset is generated between the counterpropagating directions, which will vary with changes in modulation, or cavity, parameters.

Another problem caused by asymmetry is that the quadrature signal from the PSD is not zero at the center of the effective cavity resonance. It is important to note that for a symmetric resonance, the quadrature signal from the PSD is always zero at the center of the resonance, hence changes in the phase of the PSD do not cause any offset errors. In contrast, with a non-zero quadrature, changes in the PSD phase will cause gyro offsets.

Further, the magnitude of the quadrature offset is influenced by a number of factors including modulation rate and depth, as well as cavity backscattering. Thus, even if the phase of the PSD is constant, offset errors can be generated due to quadrature variations.

Several possible methods of minimizing the errors due to lineshape asymmetry are being explored including careful selection of modulation para-

<sup>10</sup> G.A. Sanders, M.G. Prentiss, and S. Ezekiel, "Passive Ring Resonator Method for Sensitive Inertial Rotation Measurements in Geophysics and Relativity," *Opt. Lett.* 7: 569 (1981).

<sup>11</sup> F. Aronowitz, "The Laser Gyro," in *Laser Applications*, ed. M. Ross (New York: Academic Press, 1971).

<sup>12</sup> K. Iwatsuki, K. Hotate, and M. Higashiguchi, "Effect of Rayleigh Backscattering in an Optical Passive Ring-resonator Gyro," *Appl. Opt.* 23: 3916 (1984).

meters and the use of multiple modulation frequencies. However, by using a cavity in transmission, there is no lineshape asymmetry and these errors can be avoided.

Another important source of error is polarization driven. A ring cavity can, in general, support two eigen polarizations which typically have different resonance frequencies, and for maximum resonance size, the input beam is usually matched into one of these eigen polarizations. However, if the second eigen polarization is partially excited, it will pull the resonance frequency of the main polarization. If the input polarizations are exactly the same in the two directions, these resonance pulls will be the same in each direction, but if the polarizations are not matched, the pulls will cause a gyro offset. Further, if the eigen polarizations are not exactly orthogonal, or if there are polarization sensitive elements after the cavity, the resonance pulls can be greatly enhanced.

Several solutions to these polarization-driven errors are possible. First, eliminating the second eigen polarization by the use of a single polarization fiber resonator will eliminate the polarization cross talk problems. Second, the input polarization can be actively locked to a cavity eigen polarization ensuring that the input polarizations are the same in both directions and that they are exactly matched into an eigen polarization. Third, cavities made from polarization maintaining fiber with a 90 degree rotated splice have eigen polarizations that are spaced by exactly half a cavity free spectral

range.<sup>13</sup> This nulls the neighboring line resonance pull and greatly improves the temperature sensitivity of the eigen polarizations as compared to a standard polarization preserving fiber resonator.

Finally, the optical Kerr effect,<sup>14</sup> which causes a nonreciprocal phase shift due to a mismatch in the counterpropagating intensities, influences both the cavity in reflection and the cavity in transmission.

## 1.2 Stimulated Brillouin Fiber Laser Gyroscope

### Sponsor

Charles S. Draper Laboratories  
Contract DL-H-418468

Research is in progress on a new fiber optic ring laser gyroscope. This gyroscope is based on two counterpropagating stimulated Brillouin scattering (SBS) lasers<sup>15</sup> in the same single-mode fiber optic ring resonator. In the presence of inertial rotation normal to the plane of the resonator, a difference frequency is automatically generated between the counterpropagating SBS lasers which is directly proportional to the rotation,<sup>16</sup> as predicted by the Sagnac effect.<sup>17</sup> The operation of such a gyro is very similar to that of the bulkoptic ring laser gyro (RLG) that is based on two counterpropagating He-Ne lasers that share the same ring resonator.<sup>18</sup> Unlike the passive interferometric fiber gyro,<sup>19</sup> the SBS fiber gyro does not require external means for

<sup>13</sup> G.A. Sanders, R.B. Smith and G.F. Rouse, "Novel Polarization Rotating Ring Resonator for Rotation Sensing," *Proc. SPIE*, 1169 (Bellingham, Washington: SPIE, 1989), pp. 1169-74; Fiber Optic and Laser Sensors VII Conference, Boston, Massachusetts, September 5-7, 1989.

<sup>14</sup> S. Ezekiel, J.L. Davis, and R. Hellwarth, "Intensity Dependent Nonreciprocal Phase Shift in a Fiberoptic Gyroscope," in *Fiber Optic Sensors*, eds. S. Ezekiel and H.J. Arditty (Berlin: Springer-Verlag, 1982), p. 332.

<sup>15</sup> S.P. Smith, F. Zarinetchi, and S. Ezekiel, "Fiberoptic Ring Laser Gyro," *Proceedings of OFS '89*, Paris, France, 1989.

<sup>16</sup> P.J. Thomas, H.M. van Driel, and G.I.A. Stegeman, "Possibility of Using an Optical Fiber Brillouin Ring Laser for Inertial Sensing," *Appl. Opt.* 19: 1906 (1980); K.O. Hill, B.S. Kawasaki, and D.C. Johnson, "cw Brillouin Laser," *Appl. Opt. Lett.* 28: 608 (1976); D.R. Ponikvar and S. Ezekiel, "Stabilized Single-frequency Stimulated Brillouin Fiber Ring Laser," *Opt. Lett.* 6: 398 (1981); L.F. Stokes, M. Chodorow, and H.J. Shaw, "All-fiber Stimulated Brillouin Ring Laser with Submilliwatt Pump Threshold," *Opt. Lett.* 7: 509 (1982); P. Bayvel and I.P. Giles, "Evaluation of Performance Parameters of Single-mode All-fiber Brillouin Ring Lasers," *Opt. Lett.* 14: 581 (1989); F. Zarinetchi, S.P. Smith, and S. Ezekiel, "Stimulated Brillouin Fiber-optic Laser Gyroscope," *Opt. Lett.* 16: 229 (1991).

<sup>17</sup> A.H. Rosenthal, "Regenerative Circulatory Multiple Beam Interferometry for the Study of Light Propagation Effects," *J. Opt. Soc. Am.* 52: 1143 (1962).

<sup>18</sup> W.M. Macek and D.T.M. Davis, Jr., "Rate Sensing with Travelling Wave Ring Laser," *Appl. Phys. Lett.* 2: 67 (1963).

<sup>19</sup> V. Vali and L.W. Shorthill, "Fiber Ring Interferometer," *Appl. Opt.* 15: 1099 (1976).

the measurement of nonreciprocal phase shifts induced by rotation.

Figure 2 shows a simplified schematic diagram of a SBS fiber laser gyroscope. Light from a 2 mW He-Ne laser at  $1.15 \mu\text{m}$  is split into two beams, labelled P1 and P2, which are frequency shifted by acousto-optic (A/O) modulators. The beams are then coupled into counterpropagating directions of a single mode, fiber optic resonator which is 25 meters long, has a finesse of 250, and is wrapped around a 7.5 cm cylindrical drum. For maximum effective pump power in the resonator, beam P1 is held at the center of a cavity resonance using a servo loop, not shown in the figure.

With the pump input power about  $60 \mu\text{W}$ , the SBS threshold for this cavity, SBS lasers B1 and B2, which are pumped by P1 and P2 respectively, are observed. These SBS lasers outputs are combined and fall on detector D.

Figure 3a shows the difference frequency between B1 and B2, when a sinusoidal rotation is applied to the cavity, and figure 3b shows the corresponding rotation angle. As seen in the figure, the difference frequency varies linearly with the rotation rate, as predicted by the Sagnac effect, and hence is 90 degrees out of phase with the rotation angle in figure 3b. However, it is important to notice that for a range of low rotation rates, i.e., when the rotation angle near its maximum or minimum values, the beat frequency goes to zero, demonstrating the so called "lock-in" zone that is caused by the coupling of the counterpropagating lasers through backscattering inside the resonator. Lock-in, which has been extensively studied in the bulkoptic He-Ne RLG, must be removed to achieve high precision measurements.

One method of removing lock-in in the SBS fiber gyro is to mechanically dither the gyro in the same manner as the bulkoptic RLG.<sup>20</sup> However, with a SBS gyro, it is possible to avoid lock-in completely by generating the counterpropagating lasers in different longitudinal modes of the cavity. In this way, backscattering within the cavity cannot couple the SBS lasers, since the lasers are at different frequencies. For example, to separate the SBS lasers by 12 longitudinal modes, i.e.,  $\Delta q = 12$ , the frequency of pump P1 is shifted with respect to P2 by 12 free spectral ranges (FSR) using the A/O modulators shown in figure 2.

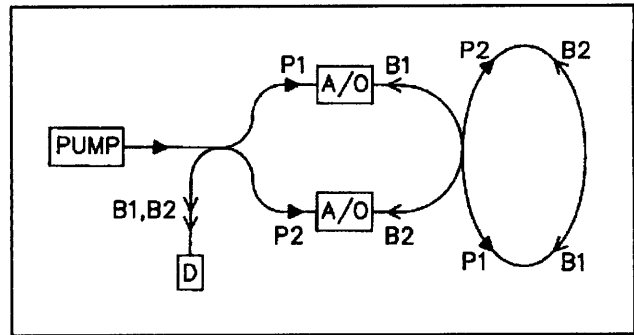


Figure 2. Simplified schematic of a SBS fiber ring laser gyroscope.

Figure 4a shows the frequency difference between the SBS lasers with  $\Delta q = 12$  and a sinusoidal rotation applied to the cavity, and figure 4b shows the corresponding rotation angle. Similar to  $\Delta q = 0$ , the change in the difference frequency between the lasers is directly proportional to the applied rotation rate. However, in this case there is no lock-in zone for low rotation rates, and the difference frequency smoothly follows the applied rotation rate. In addition, the difference frequency is not zero for zero rotation, but is at a fixed frequency offset that, in this case, corresponds to 12 FSRs, or 92.4 MHz.

There are a number of factors that influence the stability of this offset that are being investigated. Some of these include temperature, fiber birefringence, backscattering, optical Kerr effect, and dispersion pulls.

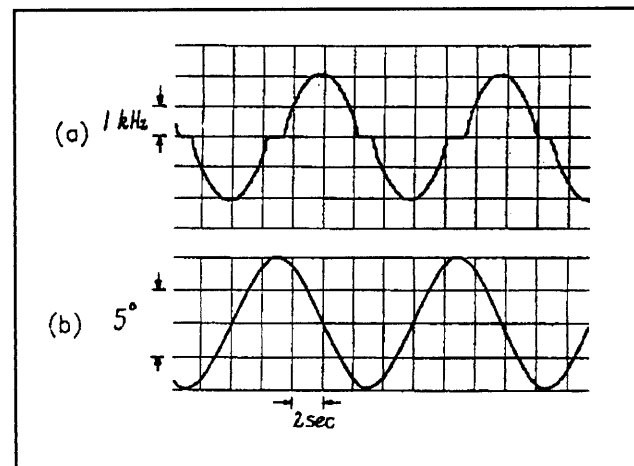
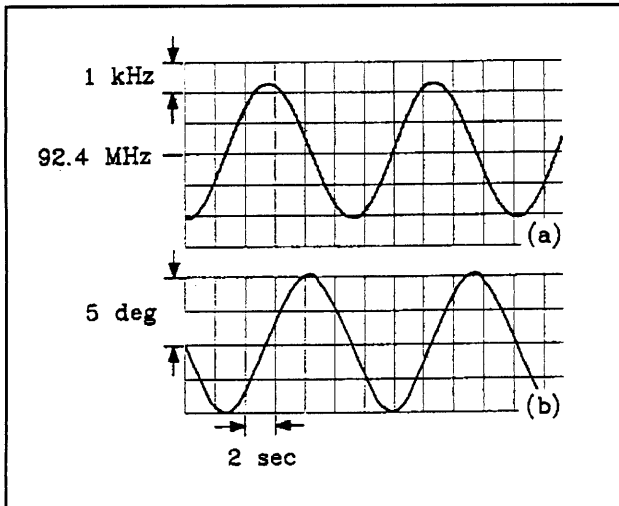


Figure 3. Simultaneous recording of (a) difference frequency between SBS lasers and (b) angle of the applied rotation.

<sup>20</sup> F. Aronowitz, "The Laser Gyro," in *Laser Applications*, ed. M. Ross (New York: Academic Press, 1971).





**Figure 4.** Simultaneous recording for  $\Delta q = 12$  of (a) difference frequency between SBS lasers and (b) angle of the applied rotation.

### 1.3 Applications of Stimulated Brillouin Fiber Lasers

#### Sponsor

Charles S. Draper Laboratories  
Contract DL-H-418468

The development of low threshold stimulated Brillouin scattering (SBS) fiber lasers has created a variety of fiberoptic devices and sensors for a wide range of applications.

Briefly stated, stimulated Brillouin scattering<sup>21</sup> is a nonlinear process in which an intense beam of light, the pump, propagating in a single mode fiber generates gain for a counterpropagating beam, the SBS beam, which is downshifted in frequency from the pump by  $(2v_a/c)f_p$ , where  $v_a$  is the speed of sound in the fiber,  $c$  is the speed of light in the fiber, and  $f_p$  is the frequency of the pump light. For example, for a pump wavelength of  $1 \mu\text{m}$  in quartz,

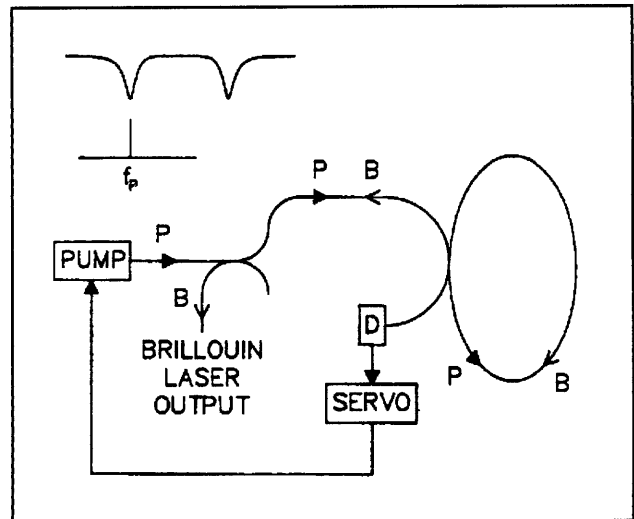


**Figure 5.** Simplified schematic of a SBS fiber ring laser.

the center of the Brillouin gain is downshifted by about 15 GHz.

The pump power needed to achieve SBS can be greatly reduced by generating the SBS inside a fiber ring cavity, as illustrated in figure 5. By holding the pump, in the direction labelled P, at the center of a cavity resonance by the use of a servo, the pump power inside the resonator can be enhanced. If the resulting round trip SBS gain is greater than the cavity losses, SBS lasing will occur along the direction opposite to that of the pump,<sup>22</sup> labelled B in the figure. The absolute linewidth of the SBS laser was shown to be less than 1 kHz,<sup>23</sup> and with better acoustic and thermal isolation, this linewidth can be further reduced.

Since the SBS laser is downshifted in frequency from the pump, it can be used as a simple, wide-band frequency shifter. A large frequency shift with respect to the pump, 15 GHz with a  $1 \mu\text{m}$  pump, can be achieved without requiring sophisticated wideband electronics. Only a relatively simple servo is needed to hold the pump laser near the center of a cavity resonance. Moreover, even

<sup>21</sup> R.Y. Chiao, C.H. Townes, and B.P. Stoicheff, "Stimulated Brillouin Scattering and Coherent Generation of Intense Hypersonic Waves," *Phys. Rev. Lett.* 12: 592 (1964).

<sup>22</sup> K.O. Hill, B.S. Kawasaki, and D.C. Johnson, "cw Brillouin Laser," *Appl. Opt. Lett.* 28: 608 (1976); D.R. Ponikvar and S. Ezekiel, "Stabilized Single-frequency Stimulated Brillouin Fiber Ring Laser," *Opt. Lett.* 6: 398 (1981); L.F. Stokes, M. Chodorow, and H.J. Shaw, "All-fiber Stimulated Brillouin Ring Laser with Submilliwatt Pump Threshold," *Opt. Lett.* 7: 509 (1982).

<sup>23</sup> S.P. Smith, F. Zarinetichi, and S. Ezekiel, "Narrow Linewidth Stimulated Brillouin Fiber Laser and Applications," *Opt. Lett.* 16: 393 (1991).

larger frequency shifts may be generated using higher order SBS lasers.<sup>24</sup>

There are also many applications for two SBS lasers generated in the same resonator, as shown in figure 6. In the figure, two independent pump lasers, in the directions labelled P1 and P2 respectively, are coupled into opposite directions of the same ring cavity and locked to different longitudinal modes of the cavity, using servos not shown in the figure. The corresponding SBS lasers, in the directions labelled B1 and B2, will have approximately the same frequency separation as the pump lasers. However, the beat between the SBS lasers will be very narrow, since they share the same cavity, and any fluctuations in the optical length of the cavity are common to both lasers.

Figure 7 shows an example of such a beat between two SBS lasers, centered at 507 MHz, which has been detected and is displayed on an electronic spectrum analyzer. The observed linewidth of 30 Hz was limited by the instrumental linewidth of the spectrum analyzer; this implies that the actual linewidth is much narrower than 30 Hz and should be close to the Schawlow-Townes limit. In contrast, the corresponding beat between the pump lasers, which were intentionally jittered, was almost 100 kHz. Thus, the beat between the two lasers can be detected and used as a microwave, or even millimeter wave source, limited only by the detector response and the tunability of the pump lasers.

SBS lasers also have a number of other applications in, for example, the generation of wideband amplitude modulated laser beams for use in absolute distance and ranging measurements. These lasers can also be used to generate two laser sources with correlated frequency jitter for fast flow laser Doppler velocimeters (LDV) and high resolution, two-photon interactions for the development of atomic clocks.

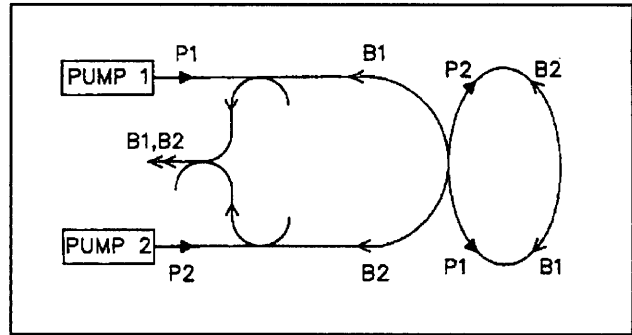


**Figure 6.** Simplified schematic of common cavity SBS lasers.

There are also a number of sensor applications for common cavity SBS lasers that take advantage of their narrow beat. An immediate application of SBS lasers is in the development of a fiber ring laser gyroscope,<sup>25</sup> which takes advantage of the directionality of the SBS gain to generate two counterpropagating SBS lasers at the same frequency in a single cavity.

In addition to the fiber ring laser gyroscope, common cavity SBS lasers open the way for a new class of fiber optic sensors.<sup>26</sup> For example, by generating the SBS laser separated by an integer number of cavity free spectral ranges, it is possible to measure temperature in an inherently digital method that does not require a "reference arm." The change in the beat frequency between the SBS lasers is directly proportional to the change in temperature, with the scale factor determined by the frequency separation of the lasers and the temperature coefficient of the optical length of the fiber cavity. Thus, by changing the frequency spacing of the SBS lasers, the scale factor of the sensor can be adjusted. This concept may also be extended to measurement of other physical quantities such as magnetic and electric fields, acceleration, and acoustics.

<sup>24</sup> S.P. Smith, F. Zarinetchi, and S. Ezekiel, "Narrow Linewidth Stimulated Brillouin Fiber Laser and Applications," *Opt. Lett.* 16: 393 (1991).

<sup>25</sup> F. Zarinetchi, S.P. Smith, and S. Ezekiel, "Stimulated Brillouin Fiber-optic Laser Gyroscope," *Opt. Lett.* 16: 229 (1991).

<sup>26</sup> S.P. Smith, F. Zarinetchi, and S. Ezekiel, "Stimulated Brillouin Scattering Fiber Laser for Novel Fiber Sensor Applications," *Proceedings of the OFS '92*, Monterey, California, 1992.

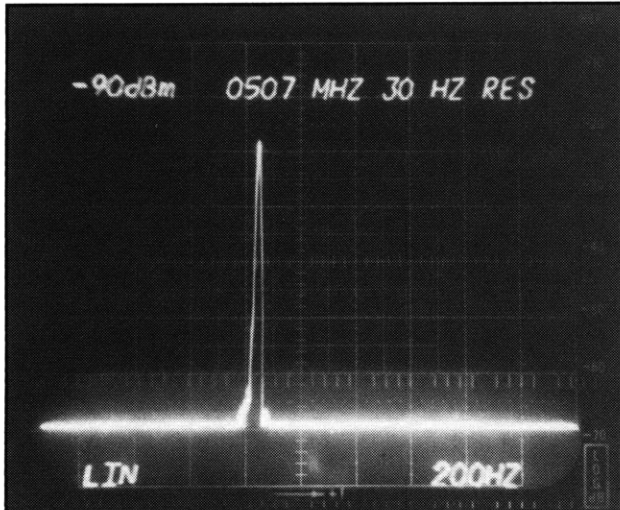


Figure 7. Spectrum of beat note between two common cavity SBS lasers centered at 507 MHz.

## 1.4 First Observation of Deflection and Cooling of Three-level Atoms in Raman Resonant Standing Wave Optical Fields

### Sponsors

U.S. Air Force - Electronic Systems Division  
Contract F19628-89-K-0300  
U.S. Navy - Office of Naval Research  
Grant N0014-91-J-1808

The interaction of two laser fields with a three-level atom in the  $\Lambda$  configuration has been of increasing interest in recent years. The force due to two counter-propagating traveling waves has already cooled such atoms below the single photon recoil limit.<sup>27</sup> Recently, theoretical solutions have shown that the force on a stationary three-level atom in standing wave fields is unbounded, with spatial variations on length scales both much longer and much shorter than an optical wavelength.<sup>28</sup> Here we show experimental verification of the existence of the long-range component of this force by deflecting an atomic beam of three-level sodium atoms using two Raman resonant

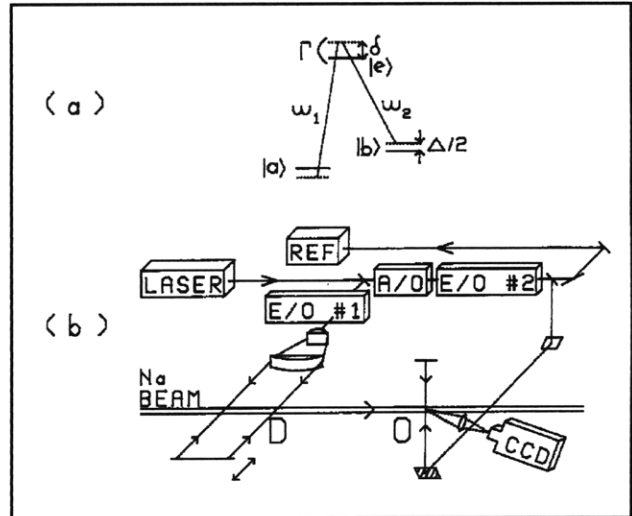


Figure 8. (a) Schematic of the three-level  $\Lambda$  system. (b) Perspective diagram of the experimental setup used to observe atomic beam deflection.

standing wave laser fields. In addition, we show the existence of damping forces.

These observations open the possibility of developing an all-optical, deep neutral atom trap with a stimulated restoring force. Most atoms in a Raman trap would be in the ground states, so that the collisional lifetime of the atoms would be much longer than in magneto-optic traps. As a result, the Raman force could ultimately lead to high densities of cold and dark atoms in traps. Such a dense collection of atoms in transparent superposition states could find applications as novel, low intensity nonlinear optical materials.<sup>29</sup> Moreover, a Raman trap could be directly used as a Raman-atomic clock, since the dark state is not light shifted.<sup>30</sup>

A schematic diagram of the three-level  $\Lambda$  system is shown in figure 8a. The experimental setup used to observe deflection of a sodium atomic beam is shown schematically in figure 8b. Atomic beam deflection data obtained with the setup of figure 8 are shown in figure 9. For this data we chose to use the maximum laser power available ( $200 \text{ mW/cm}^2$ ) in the deflection zone. The detunings were then optimized ( $\Delta = -16 \text{ MHz}$ ,

<sup>27</sup> A. Aspect, E. Arimondo, R. Kaiser, N. Vansteenkiste, and C. Cohen-Tannoudji, *Phys. Rev. Lett.* 61: 826 (1988).

<sup>28</sup> S. Shahriar, P.R. Hemmer, N.P. Bigelow, and M.G. Prentiss, Quantum Electronics and Laser Science Conference, May 1991; M.G. Prentiss, N.P. Bigelow, S. Shahriar, and P.R. Hemmer, *Opt. Lett.* 16: 1695 (1991).

<sup>29</sup> S. Shahriar and P.R. Hemmer, *Phys. Rev. Lett.* 65: 1865 (1990).

<sup>30</sup> P.R. Hemmer, S. Shahriar, V.D. Natoli, and S. Ezekiel, *J. Opt. Soc. Amer. B* 6: 1519 (1989).

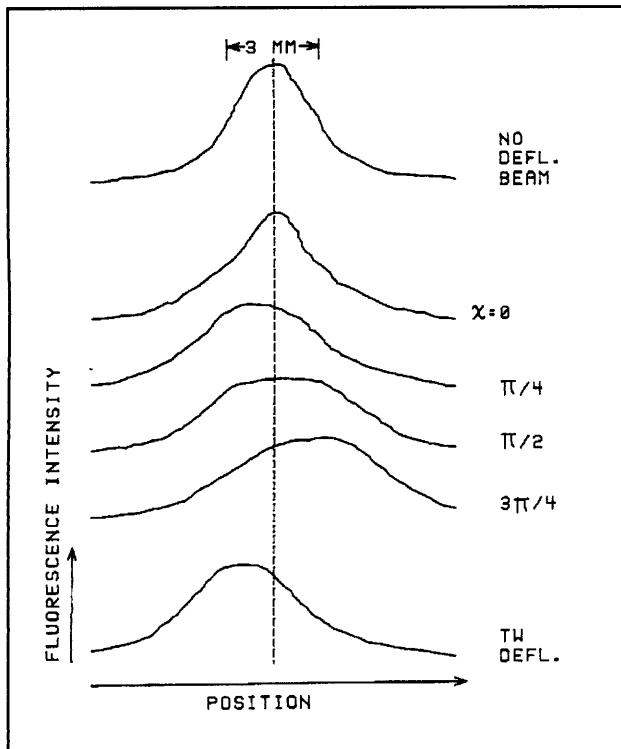


**Figure 9.** Data showing atomic beam deflection. Traces are obtained by digitizing single lines of stored video images.

$\delta = 4.4$  MHz) to observe the cleanest deflection. Here, the top trace shows the atomic beam profile with the deflecting laser blocked. The next four traces show the deflection obtained for standing wave fields having relative phase shifts of  $\chi = 0, \pi/4, \pi/2,$  and  $3\pi/4$  as labeled. Finally, the bottom trace in the figure is obtained with the retroreflected deflecting laser beam blocked showing the spontaneous deflection. As can be seen, the deflection basically behaves as  $\sin(2\chi)$ . When the value of  $\Delta$  is reversed, the stimulated deflection is reversed at every value of  $\chi$ , while the spontaneous deflection remains unchanged. These observations are in qualitative agreement with theoretical prediction.

As we have pointed out, the deflection force changes sign when the sign of  $\Delta$  is reversed. This property can be helpful in designing an all-optical trap. Briefly stated, one can conceivably design a

B-field gradient such that the value of  $\Delta$  is anti-symmetric with respect to the zero field point, which would be the trap center. Of course, in order for such a trap to work, one would need a mechanism for cooling. We have performed numerical calculations for the friction force and have found evidence that, when averaged over an optical wavelength, it varies strongly as a function of  $\chi$ . We have found experimental evidence (not shown) of such phase dependent cooling, being at its maximum at the phase where the deflection is at maximum.

In summary, we have observed the phase dependent deflection and cooling of a sodium atomic beam by two standing waves simultaneously near resonance with both components of a  $\Lambda$  three-level system. Qualitative agreement between theory and experiment is achieved. Potential applications to high-density, dark atom traps are currently being investigated. Such dark atom traps may be useful in nonlinear optics and as a Raman-atomic clock.

## 1.5 Origin of the Optical Force on the Raman Dark State in Two Standing Waves

### Sponsors

U.S. Air Force - Electronic Systems Division  
Contract F19628-89-K-0300

U.S. Navy - Office of Naval Research  
Grant N0014-91-J-1808

Recently, the optical force on three-level atoms has been investigated for several promising applications. The force associated with coherent population trapping due to counterpropagating traveling wave fields has cooled atoms below the single photon limit.<sup>31</sup> On the other hand, three-level atoms in two standing waves have been cooled as well as deflected, with potential applications to a novel, high density trap.<sup>32</sup> There have been disparate calculations of the force on an atom in two standing wave excitation fields,<sup>33</sup> which have not discussed the underlying physical processes in any detail. Here we describe the origin of the force on stationary atoms in terms of the evolution of the

<sup>31</sup> A. Aspect, E. Arimondo, R. Kaiser, N. Vansteenkiste, and C. Cohen-Tannoudji, *Phys. Rev. Lett.* 61: 826 (1988).

<sup>32</sup> P. Hemmer, S. Shahriar, M. Prentiss, D. Katz, K. Berggren, and J. Mervis, accepted for presentation at the Quantum Electronics and Laser Science Conference, 1992.

<sup>33</sup> J. Javanainen, *Phys. Rev. Lett.* 64: 519 (1990); S. Chang, B.M. Garraway, and V.G. Minogin, *Opt. Comm.* 77: 19 (1990).

normal modes of the atom field system.<sup>34</sup> We show that most of the qualitative features of the force can be derived by inspection without actually solving the optical Bloch equations (OBEs).

We recall<sup>35</sup> first that, in steady state, the Raman system is in the dark state as long as  $\Delta$ , the difference detuning (see figure 8a), vanishes. To take advantage of this, we choose to express the Raman interaction in a representation wherein the dark state is one of the basis states. For non-zero but small values of  $\Delta$ , the Raman interaction can then be represented as a perturbative excitation into states that are orthogonal to the dark state. We find that if  $\delta$ , the common detuning (see figure 8a) vanishes, the optical force is only on the dark state, thus further simplifying the analysis.

To start with, we restrict the calculation to the regime wherein the Rabi frequencies are much weaker than the natural lifetime. This allows us to eliminate the excited state by invoking the adiabatic following approximation.<sup>36</sup> We are then left with a two-level system coupled by  $\Delta$ . This problem is then solved perturbatively, since  $\Delta$  is assumed to be small. The resulting expression for the optical force on a three-level system for the case of two standing waves with equal amplitudes and a phase difference of  $\pi/4$  is illustrated in figure 10. Figure 10a shows the Rabi frequencies. The force expression is plotted and compared to the exact solution of the optical Bloch equations (OBEs) in figure 10b. The solid curve is a plot of the perturbative estimate, and the circles correspond to the OBE solution. The lowest order force estimate agrees well with the OBE result. However, unlike the OBE solution, the perturbative solution can be interpreted physically, enabling us to understand the origin of the sharp structures.

Not only does the force in the  $\Lambda$  system show sub-optical-wavelength behavior, but it can show strong rectification (i.e., non-zero value when averaged over an optical wavelength). One case in which the origin of this rectification can be clearly illustrated is when  $\Delta$  is large, so that the reduced two level interaction is saturated. The force expression in this case can also be found by

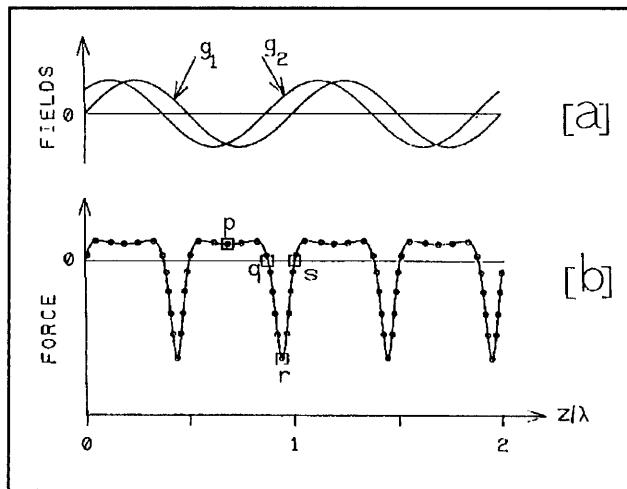


**Figure 10.** (a) The Rabi frequencies. (b) Sub wavelength structure in the optical force, computed by a perturbative estimate (solid line), and compared with the exact solution of the optical Bloch Equations (circles).

mere inspection, as is illustrated in figure 11. The rectified component of this force as a function of  $\chi$ , the phase difference between the standing waves, is shown by the solid line. The dotted curve is the rectified force computed using the exact solution of the OBEs. Again, there is reasonably good agreement.

To summarize, we have used the normal modes of the atom field to physically model the origins of novel structures that appear in the force on a  $\Lambda$  system atom under standing wave excitation. In particular, we have identified a situation where the force is only on the dark state, thus leading to simple, closed form expressions for the force. Finally, our estimated results agree well with solutions of the OBEs in the regions where the approximations used are valid. Future work will involve using the normal modes of the atom-field system to model phase  $\chi$  dependent cooling.

We are grateful to AT&T Bell Laboratories and the Laboratory for Laser Energetics (LLE) in Rochester, New York for their support of this project.

<sup>34</sup> H.R. Gray, R.M. Whitley, and C.R. Stroud, Jr., *Opt. Lett.* 3: 218 (1978).

<sup>35</sup> P.R. Hemmer, G.P. Ontai, and S. Ezekiel, *J. Opt. Soc. Amer. B* 3: 219 (1986).

<sup>36</sup> P.R. Hemmer and M.G. Prentiss, *J. Opt. Soc. Amer. B* 5: 1613 (1988); P.R. Hemmer, M.S. Shahriar, V.D. Natoli, and S. Ezekiel, *J. Opt. Soc. Amer. B* 6: 1519 (1989).

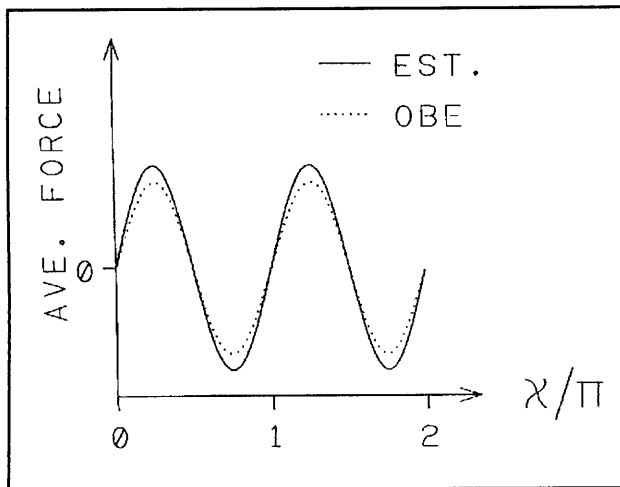


**Figure 11.** Wave-length averaged force as a function of the standing wave phase difference, computed by a perturbative estimate (solid line), and compared with the exact solution of the optical Bloch Equations (dotted line).

### Publications

Hemmer, P., M. Prentiss, and S. Shahriar. "Optical Force on the Raman Dark State in Two Standing Waves." *Opt. Commun.* Forthcoming.

Prentiss, M., N. Bigelow, S. Shahriar, and N. Bigelow. "Forces on Three Level Atoms Including Coherent Population Trapping." *Opt. Lett.* 16: 1695 (1991).

Prentiss, M.G., N. Bigelow, M.S. Shahriar, P.R. Hemmer, K. Berggren, J. Mervis, S. Ezekiel. "Laser Manipulation of Atoms and Ions." Enrico Fermi International School of Physics, Course CXVIII. Milan, Italy, July 1991.

Shahriar, S., P. Hemmer, N. Bigelow, and M. Prentiss. "Forces on Three Level Atoms Including Trapped State Contribution." In *Quantum Electronics and Laser Science*. Technical Digest Series. Washington, D.C.: Optical Society of America, 1991. pp. 186.

## 1.6 Optical Data Storage with Raman Excited Microwave Spin Echoes

### Sponsor

U.S. Air Force - Electronic Systems Division  
Contract F19628-89-K-0030

Recently, there has been a great deal of interest in the use of optical photon echoes for information storage and processing.<sup>37</sup> However, so far experimental demonstrations have been restricted to spectral hole burning materials operating at liquid He temperatures. Information has been stored using microwave spin echoes in room temperature materials,<sup>38</sup> but the data rates and storage densities achievable are orders of magnitude below those of optical echo techniques. The proposed scheme, which makes use of an optically excited microwave spin echo, is capable of data rates and storage densities comparable to optical echo techniques, but potentially at much higher temperatures (provided a suitable material can be found). In contrast to multilevel optical echoes, the Raman excited microwave coherences could store information which is spread over times much longer than the homogeneous decay time of the optical coherence.

The basic architecture of the proposed scheme is illustrated in figure 12. A three-level system is used, which can be excited by two near resonant optical transitions (resonance Raman) or one near resonant microwave transition (see figure 8a). As shown, information is first input as an optical pulse train (two unequal amplitude pulses in the figure). The optical input beam contains both optical frequencies needed to excite the resonance Raman transition. The Raman interaction creates a coherence which depends on phase differences in the two optical frequencies. This phase sensitivity, combined with dephasing of the ground state coherence due to inhomogeneous broadening, allows both the temporal and phase information contained in the optical fields to be stored via a process analogous to spectral hole burning. To recall this information, a  $\pi$ -pulse must be applied. Since the Raman coherence directly translates into a microwave coherence<sup>39</sup> this can be accomplished with a microwave  $\pi$ -pulse. The ground state

<sup>37</sup> M.K. Kim and R. Kachru, "Storage and Phase Conjugation of Multiple Images Using Backward-stimulated Echoes in  $\text{Pr}^{3+}:\text{LaF}_3$ ," *Opt. Lett.* 12: 593 (1987).

<sup>38</sup> S. Fernbach and W.G. Proctor, "Spin-echo Memory Device," *J. Appl. Phys.* 26: 170 (1955).

<sup>39</sup> M.S. Shahriar and P.R. Hemmer, "Direct Excitation of Microwave-spin Dressed States Using a Laser-excited Resonance Raman Interaction," *Phys. Rev. Lett.* 65: 1865 (1990).

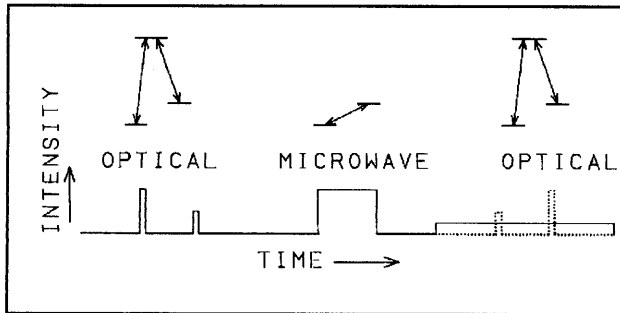


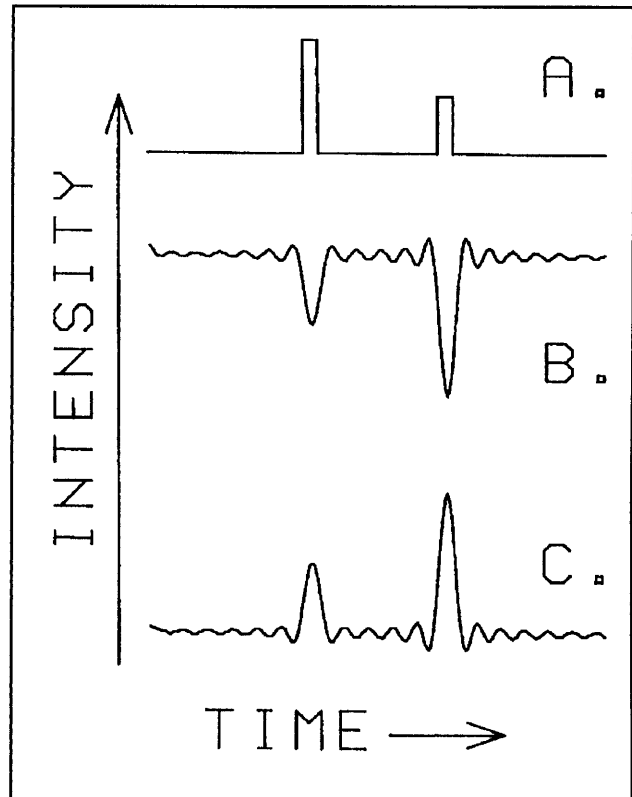
**Figure 12.** Schematic showing proposed architecture for optical data storage with Raman-microwave spin echoes. The dotted lines on the right side show the microwave spin echoes which are detected by an optical Raman probe (superimposed solid line).

coherences will then rephase at the appropriate time where they can be detected optically, as bright and dark areas, using an optical Raman probe, as shown in figure 12.

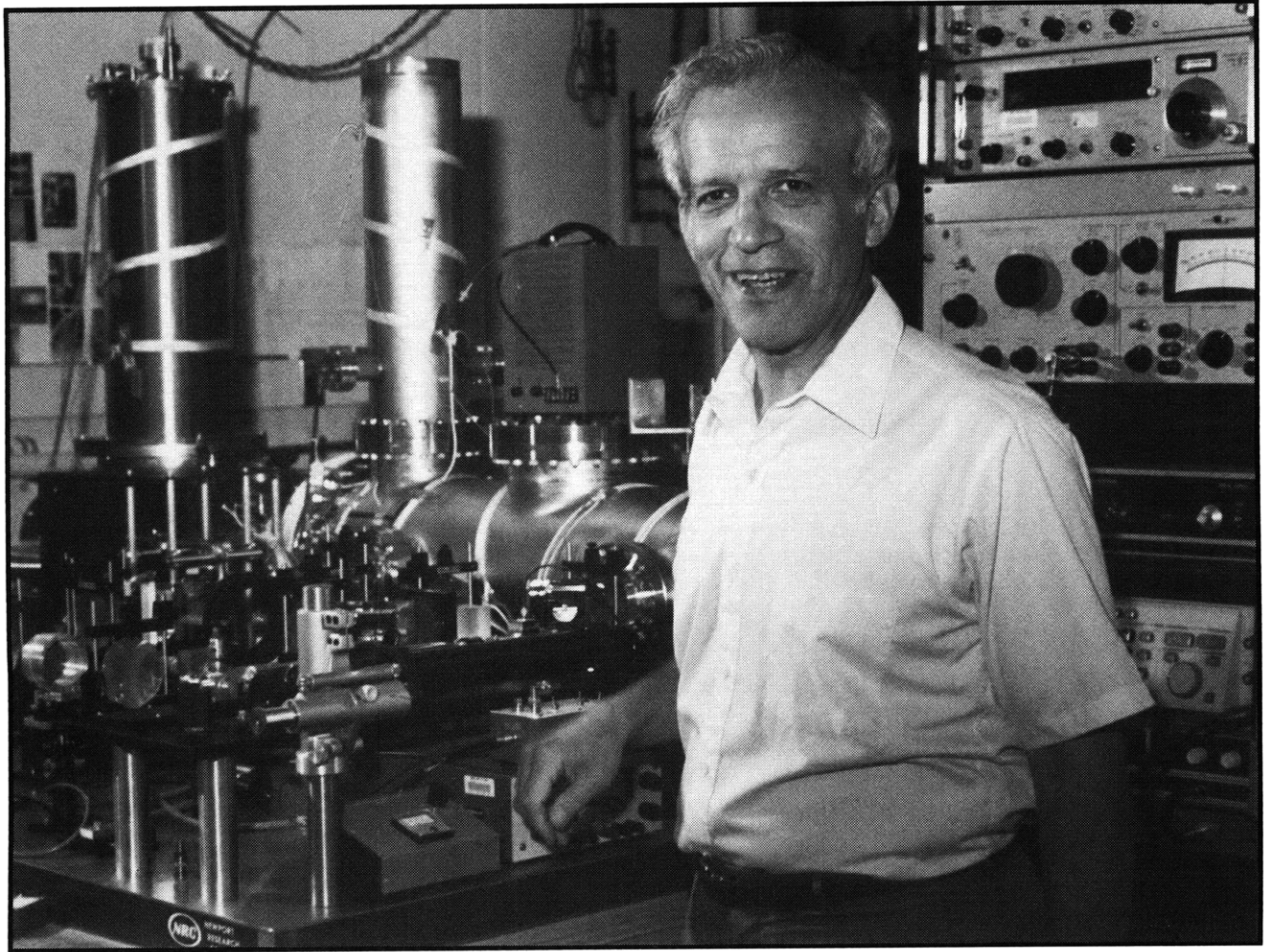
Figure 13a shows the theoretical input pulse train and figures 13b and 13c show the optically detected echo pulses for in and out of phase optical Raman probing fields, respectively. As shown, both positive and negative versions of the input information can be retrieved. These traces were produced using density matrix equations that had been developed to explain experimentally observed optical-microwave interactions.<sup>39</sup>

In summary, we have studied the process whereby resonant Raman excitation is used to store information in ground state spin-coherences that are long-lived and inhomogeneously broadened. A microwave  $\pi$ -pulse is used to rephase the coherences, so that the information can be restored via Raman detection of spin echoes. These tech-

niques promise to combine the advantages of optical echo (high resolution) and spin echo (long lived) so that photon echo based optical data storage may possibly be achieved in room temperature materials.



**Figure 13.** (a) Input optical pulse train. (b) Optically detected output microwave pulse train for in-phase Raman probe fields. (c) Output for out of phase Raman probe.



*Professor Daniel Kleppner*